An Improved Force Distribution Function for Linear Switched Reluctance Motor on Force Ripple Minimization With Nonlinear Inductance Modeling

J. F. Pan[1], Norbert C. Cheung[2], *Senior Member, IEEE*, and Yu Zou[1]

[1]Department of Automation Science, College of Mechatronics and Control Engineering, Shenzhen University, Shenzhen518060 China

[2]Department of Electrical Engineering, The Hong Kong Polytechnic University, Hunghom, Kowloon, Hong Kong, China

An improved force distribution function (FDF) of linear switched reluctance motors (LSRMs) based on nonlinear inductance modeling for force ripple minimization and smooth speed operation is proposed. Nonlinear inductance profile is divided into three segments with a K factor that depicts current effect on inductance of the LSRM. Speed controller based on the proposed FDF and the nonlinear inductance model is constructed. Both simulation and experimental results verify the proposed FDF with the nonlinear inductance modeling effectively reduce force ripples with uniform speed response.

***Index Terms*—FDF, force ripple minimization, LSRM, nonlinear inductance modeling.**

I. Introduction

LINEAR switched reluctance motors (LSRMs) have the characteristics of excellent heat dispersion, mechanical robustness and fault tolerance. With the development of power electronics and advanced algorithms [1]–[3], there have been widespread research interests in LSRMs. Compared to other linear machines such as linear alternating-current synchronous [4], linear permanent magnet [5], [6] and linear induction motors [7]–[9], LSRMs have not yet been widely applied due to their inherently high force ripples especially in low speed. For smooth speed operation of the LSRMs, total force impressed on the moving platform should remain at reasonable values with minimum fluctuations. One of the effective methods for force ripple minimization is to obtain a reasonable force distribution function (FDF) for the LSRM. Previous attempts focus on linear or sinusoidal FDFs [10], and treat the inductance profiles linearly, neglecting saturation and current influence on inductance. The FDF proposed in [2] is derived from the change rate of inductance, limited to first or second order. The FDFs from inaccurate inductance modeling require current and velocity controller for compensation and the inaccuracy of inductance model inevitably deteriorates the control performances [11].

In this paper, an improved FDF based on nonlinear inductance modeling that considers both position and current influence is proposed. The method to obtain the optimized FDF for LSRMs is discussed. Sectional inductance modeling is employed to characterize machine nonlinearity. The nonlinear inductance profile is divided into three segments and a K factor that depicts current effect on inductance is introduced. The speed controller based on the proposed FDF with multiphase excitation scheme is constructed. Simulation is performed to evaluate force characteristics and results verify the validity on force ripple minimization. Experimental tests on speed control under different FDF schemes are obtained and compared. The experimental results demonstrate that the proposed FDF effectively reduce force ripples and the speed response exhibits fewer speed fluctuations.

Manuscript received March 01, 2012; accepted May 25, 2012. Date of current version October 19, 2012. Corresponding author: N. C. Cheung (e-mail: norbert.cheung@polyu.edu.hk).

Color versions of one or more of the figures in this paper are available online at http://ieeexplore.ieee.org.

Digital Object Identifier 10.1109/TMAG.2012.2202376

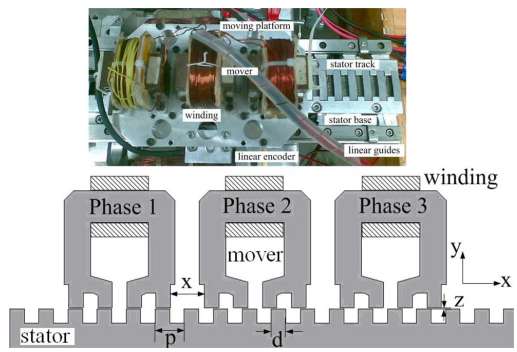

Fig. 1. Prototype and schematic of the LSRM.

II. Modeling of the LSRM

A. Structure of the LSRM

The LSRM is mainly composed of a moving platform and stator base. Three-phase movers are mounted with windings of the same dimensions and ratings and assembled on the moving platform. The moving platform translates along with a pair of linear guides and a linear encoder for real-time position information detection is installed. The stator track and the mover cores are laminated with silicon-steel plates. The moving platform and stator base are manufactured from aluminum alloy to ensure a low inertia and decoupled magnetic paths [1].

The prototype and electromagnetic structure are shown in Fig. 1. Table I lists main specifications of the LSRM.

B. Mathematical Model of the LSRM

The electrical terminal for any one phase can be characterized as the voltage balancing equation as follows:

$$u = R \cdot i + \frac{d\lambda(i,x)}{dt} \tag{1}$$

TABLE I
SPECIFICATIONS OF THE LSRM

Rated current	4 A
Mass of moving platform (M)	1.5 kg
Mass of stator (M_s)	2 kg
Pole width (d)	6 mm
Pole pitch (p)	12 mm
Phase division (x)	10 mm
Phase resistance (R)	2 ohm
Air gap length (z)	0.3 mm
Number of turns (N)	160
Stack length	25 mm
Encoder resolution	1 μm

where R, u, and i represent phase resistance, terminal voltage and current, respectively. x is displacement and $\lambda(i,x)$ denotes flux-linkage. From the mechanical side

$$F = M \cdot \frac{d^2x}{dt^2} + B \cdot \frac{dx}{dt} + f_l = \frac{\partial W_{\rm co}(i,x)}{\partial x} \tag{2}$$

where F is electromagnetic force, f_l, M and B are load force, mass of moving platform and friction coefficient, respectively. Co-energy $W_{\rm co}(i,x)$ can be further represented as

$$W_{\rm co}(i,x) = \int_0^i \lambda(i,x)di = \int_0^i L(i,x) \cdot idi. \tag{3}$$

It is clear that inductance is a function of both phase current and displacement. If the LSRM is operating in linear region, we have

$$F = \frac{1}{2} \cdot i^2 \cdot \frac{\partial L(i,x)}{\partial x}. \tag{4}$$

Equation (4) indicates that change rate of inductance respective to position and current are the key factors on force output and variations.

C. Inductance Model

The nonlinear inductance model is constructed from the following steps.

1) Inductance $L(x)$ dependent on position only is divided into three segments from the fully un-aligned to fully aligned position and each section is 2 mm.
2) Curve fitting for each section is based on the least square method. The middle part of inductance profile (2–4 mm) is represented by linear approximation and quadratic function is applied for section 0–2 mm and 4–6 mm, respectively. Then $L(x)$ can be expressed as

$$L(x) = \begin{cases} Ax^2 + Bx + C_1 \\ Dx + C_2 \\ Ex^2 + Fx + C_3 \end{cases} \tag{5}$$

Fig. 2 shows the result of polynomial fitting for $L(x)$ with $A = 0.5$, $B = 1.78$, $C_1 = 11.8$, $C_2 = 10.82$, $C_3 = 0.57$, $D = 3.22$, $E = -0.53$ and $F = 7.48$ for the LSRM.

3) A K factor that reflects the influence of current excitation is introduced. Since the machine operates in the range of 1 to 4 A, the inductance respective to both current and position $L(i,x)$ is represented as the multiplication of $L(x)$ and K as depicted in the following expressions as:

$$L(i,x) = \begin{cases} (Ax^2 + Bx + C_1) \cdot K(i,x) \\ (Dx + C_2) \cdot K(i,x) \\ (Ex^2 + Fx + C_3) \cdot K(i,x) \end{cases} \tag{6}$$

where $K(i,x) = ax^3 + bx^2 + cx + d$. Coefficient a-d reflect inductance profiles dependent on current values and can be obtained in Table II through FEM simulation with numerical fitting. Waveform of K as current value from 1 to 4 A is shown in Fig. 3 and the complete inductance profile can be found in Fig. 4.

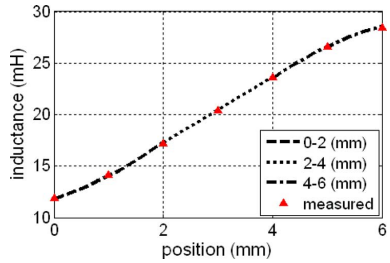

Fig. 2. Segmented inductance with curve fitting.

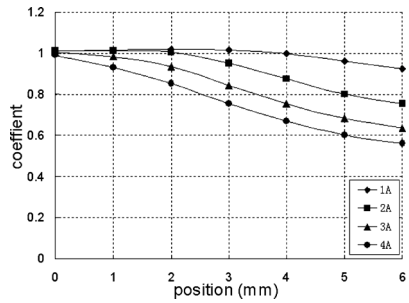

Fig. 3. K factor versus position in different current region.

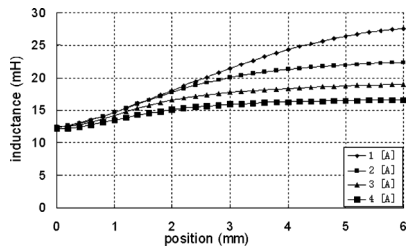

Fig. 4. Inductance profile of the LSRM versus position and current.

D. Proposed FDF

According the force generation equation denoted in (4), assuming that

$$g_n(i,x) = \frac{1}{2} \cdot \frac{\partial L(i,x)}{\partial x} \tag{7}$$

TABLE II
COEFFICIENTS' VALUE OF K

Current (A)	a	b	c	d
1	-0.000503	-0.001223	0.00988	1.01
2	0.002498	-0.03095	0.0537	0.9974
3	0.003431	-0.03401	0.02104	0.9961
4	0.002406	-0.0196	0.04068	0.9905

then phase current can be represented as

$$i_n^* = \sqrt{\frac{F_n^*}{g_n(x)}} \quad (n = 1, 2, 3) \tag{8}$$

where F_n^* is force reference of the nth phase. The relationship between total force reference F^* and F_n^* can be depicted as

$$F_n^* = F^* \cdot f_n \tag{9}$$

where f_n is the desired FDF. Extending the FDF to pth order discussed in [2], the FDF can be represented as

$$f_n = \frac{F_n^*}{F^*} = \frac{1}{1 + \left[\frac{g_{n-1}(x)}{g_n(x)}\right]^p}. \tag{10}$$

For current command between 1 to 2 A, the FDF waveform of Phase 2 at 2–4 mm and current command as p approaches infinity can be found in Fig. 5. It is clear that the change rate of FDF increases as p gets bigger. Since current drivers cannot track current command curves with large gradient accurately, for smooth current profile with reasonable peak current values, p is selected as 3.5 for the FDF of the LSRM. The complete FDF profile can be found in Fig. 5(c).

III. CONTROL STRATEGY

A. Current Control With FDF

The FDF block can be depicted as shown in Fig. 6. The FDF block first determines which phase(s) should be excited according to F^* and x. Then force command for each phase can be derived according to the complete FDF expression. Next, current reference for each phase can be calculated according (8) and the derived inductance model. Last the actual current output for each phase is generated from the current controller.

B. Speed Regulation of the LSRM

The speed control diagram can be found in Fig. 7. To prevent the moving platform from hitting stator ends, a simple but effective proportional-integral (PI) controller is employed for position range limit. The velocity controller is designed based on a proportional-integral-differential (PID) control algorithm. Under the assumption that the bandwidth of current control loop is ten times higher than that of the speed control loop, it can be regarded that current controller has perfect tracking capability and linearity [1].

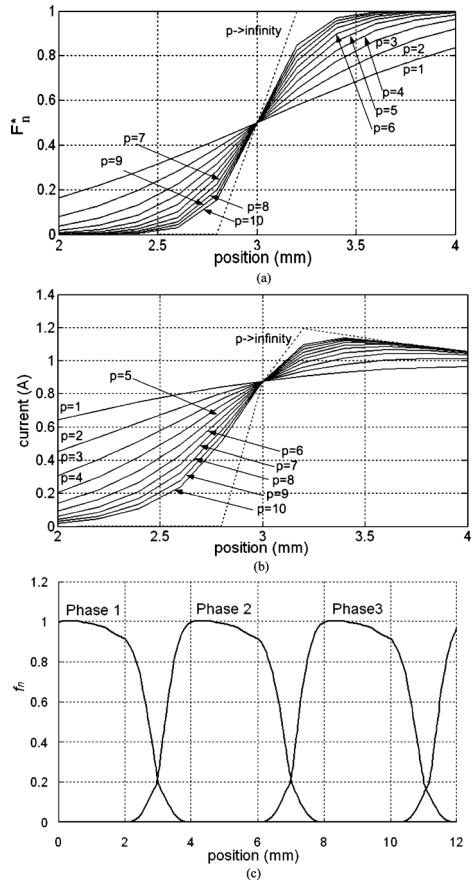

Fig. 5. (a) FDF waveform of Phase 2 (b) current command waveform as p varies from 1 to infinity and (c) complete FDF at 1–2 A.

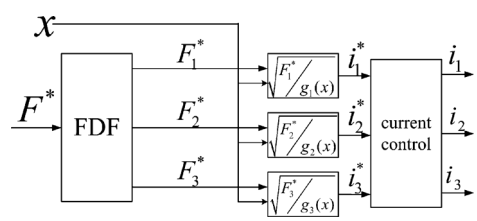

Fig. 6. FDF and current control block.

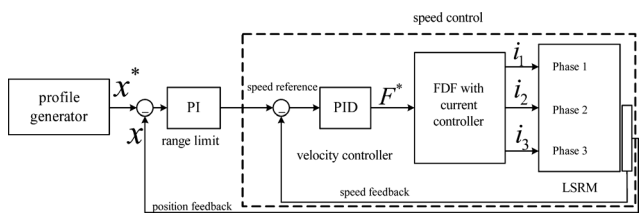

Fig. 7. Speed control diagram.

IV. SIMULATION AND EXPERIMENTAL RESULTS

A. Simulation Results

Simulation for force output of the LSRM with the proposed FDF and inductance model has been performed using *MATLAB/SIMULINK* software. The control parameters are tabulated in Table III. Force ripple waveforms from the linear, sinusoidal and the proposed FDF are drawn together in Fig. 8. It can be concluded that peak force variations appear as two phases are excited simultaneously and response from the proposed FDF

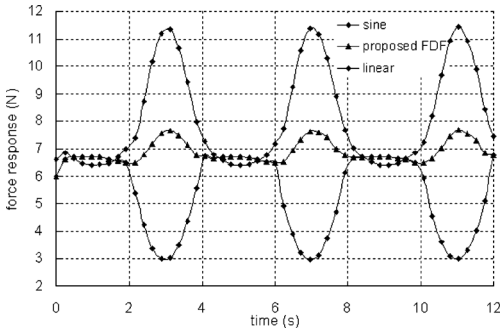

Fig. 8. Simulation results of force response at speed reference of 100 mm/s.

TABLE III
CONTROL PARAMETERS

parameter	range limit	velocity controller
P	1	0.15
I	0.9	0.08
D	0	0.002

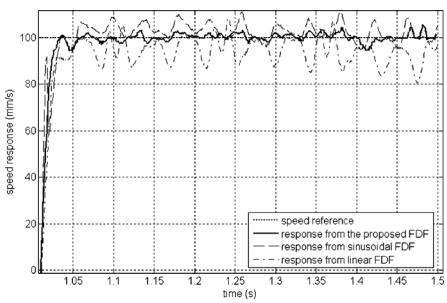

Fig. 9. Speed response under different FDFs.

with nonlinear modeling at speed reference of 100 mm/s has the least force ripples.

B. Experimental Results

Experiment on speed control is carried out based on dSPACE DS1104 controller card [1]. The whole experiment is conducted in real-time and the sampling frequency for position and velocity control loop is 1 kHz. The current controllers are commercial amplifiers capable of inner current regulation based on PI algorithm and fast enough to meet the requirements for position control loop with 20 kHz switching frequency. Experimental results of step speed response under linear, sinusoidal and the proposed FDF are illustrated in Fig. 9. With speed reference of 100 mm/s, maximum speed value is 107 mm/s and minimum value of 77 mm/s for sinusoidal and linear FDF, respectively. The speed response from the proposed FDF with segmented inductance model falls into (92.5, 100.6). It can be seen that experiment verifies the effectiveness of the proposed FDF and nonlinear modeling for smooth speed operation.

V. CONCLUSION

In this paper, nonlinear inductance model is segmented and current effect on inductance for LSRMs is discussed. By introducing the K factor, nonlinear inductance model respective to both current and position is constructed for the LSRM. The improved FDF is derived for the LSRM. Speed control system is established based on the proposed FDF and inductance model with PID control method. Simulation for force output of the LSRM under linear, sinusoidal, and the proposed FDF is presented and results verify the proposed FDF with segmented inductance model has minimum force fluctuations. Speed response from experimental results validates the effectiveness of the proposed FDF and the inductance model for smooth speed operation. It is expected that the proposed FDF and the nonlinear inductance profile contribute to accurate mathematical modeling and high-precision speed regulation of LSRMs.

ACKNOWLEDGMENT

The authors would like to thank the National Natural Science Foundation of China and Guangdong Natural Science Foundation for sponsoring of research projects under the code 51007059 and S2011010001208; the authors would also like to thank Shenzhen government JC201005280390A and ZYB200907080073A and Hong Kong Polytechnic University fund G-YXZQ for support.

REFERENCES

[1] S. W. Zhao, N. C. Cheung, W.-C. Gan, J. M. Yang, and J. F. Pan, "A self-tuning regulator for the high-precision position control of a linear switched reluctance motor," *IEEE Trans. Ind. Electron.*, vol. 54, no. 5, pp. 2425–2434, Oct. 2007.

[2] S. L. Hong, R. Krishnan, and N. S. Lobo, "Design and control of a linear propulsion system for an elevator using linear switched reluctance motor drives," *IEEE Trans. Ind. Electron.*, vol. 55, no. 2, pp. 534–542, Feb. 2008.

[3] B. Ge, A. T. de Almeida, and F. J. T. E. Ferreira, "Design of transverse flux linear switched reluctance motor," *IEEE Trans. Mag.*, vol. 45, no. 1, pp. 113–119, Jan. 2009.

[4] H.-W. Cho, H.-K. Sung, S.-Y. Sung, D.-J. You, and S.-M. Jang, "Design and characteristic analysis on the short-stator linear synchronous motor for high-speed Maglev propulsion," *IEEE Tran. Mag.*, vol. 44, no. 11, pp. 4369–4372, Nov. 2008.

[5] J. Chang, D. Kang, J. Lee, and J. Hong, "Development of transverse flux linear motor with permanent-magnet excitation for direct drive applications," *IEEE Tran. Mag.*, vol. 41, no. 5, pp. 1936–1939, May 2005.

[6] R. Cao, M. Cheng, C. Mi, W. Hua, and W. Zhao, "A linear doubly salient permanent-magnet motor with modular and complementary structure," *IEEE Trans. Mag.*, vol. 47, no. 12, pp. 4809–4821, Dec. 2011.

[7] J. X. Jin, L. H. Zheng, Y. G. Guo, and J. G. Zhu, "Performance characteristics of an HTS linear synchronous motor with HTS bulk magnet secondary," *IEEE Trans. Ind. Appl.*, vol. 47, no. 6, pp. 2469–2477, Nov./Dec. 2011.

[8] A. Z. Bazghaleh, M. R. Naghashan, and M. R. Meshkatoddini, "Optimum design of single-sided linear induction motors for improved motor performance," *IEEE Tran. Mag.*, vol. 46, no. 11, pp. 3939–3947, Nov. 2010.

[9] T. Morizane, K. Tsujikawa, and N. Kimura, "Control of traction and levitation of linear induction motor driven by power source with frequency component synchronous with the motor speed," *IEEE Tran. Mag.*, vol. 47, no. 10, pp. 4302–4305, Oct. 2011.

[10] X. D. Xue, K. W. E. Cheng, and S. L. Ho, "Optimization and evaluation of torque-sharing functions for torque ripple minimization in switched reluctance motor drives," *IEEE Tran. Power. Electron.*, vol. 24, no. 9, pp. 2076–2090, Sept. 2009.

[11] V. P. Vujičíc, "Minimization of torque ripple and copper losses in switched reluctance drive," *IEEE Tran. Mag.*, vol. 27, no. 1, pp. 388–399, Jan. 2012.